Volumetric solid concentration as a main proxy for basal force fluctuations generated by highly concentrated sediment flows

Marco Piantini[1], Florent Gimbert[2], Evangelos Korkolis[3], Romain Rousseau[4], Hervé Bellot[4], and Alain Recking[5]

[1]University Grenoble Alpes, CNRS, IRD, IGE
[2]CNRS France, Institut des Géosciences de l'Environnement
[3]University of Oslo
[4]University Grenoble Alpes, INRAE, ETNA
[5]INRAE, University Grenoble Alpes

November 22, 2022

Abstract

Sediment flows generate ground vibrations by exerting basal force fluctuations on the riverbed, which motivates the use of seismology to indirectly measure flow properties. Linking the force fluctuations and properties of highly concentrated sediment flows, however, remains particularly challenging due to complexities that arise from grain-to-grain interactions. Here we conduct downscaled flume experiments designed to investigate the influence of grain scale processes on the generation of force fluctuations for stratified sediment flows associated with significant grain sorting. We demonstrate that, under such flow conditions, the amplitude of force fluctuations decreases as the volumetric solid concentration increases. We suggest that this dependency reflects the negative relationship between volumetric solid concentration and particle agitation, which in turn controls the amplitude of force fluctuations. We therefore advance that volumetric solid should be incorporated in seismic models as a key parameter describing the particle agitation of highly concentrated sediment flows.

Volumetric solid concentration as a main proxy for basal force fluctuations generated by highly concentrated sediment flows

M. Piantini[1,2], F. Gimbert[1], E. Korkolis[1], R. Rousseau[2], H. Bellot[2] and A. Recking[2]

[1]University Grenoble Alpes, CNRS, IRD, Institute for Geosciences and Environmental Research (IGE), Grenoble, France.

[2]University Grenoble Alpes, INRAE, ETNA, Grenoble, France.

Corresponding author: Marco Piantini (marco.piantini@tiscali.it)

Key Points:

- We investigate the seismic signature of laboratory highly concentrated flows exhibiting rheological stratification and grain sorting
- We observe a negative relationship between the volumetric solid concentration and the amplitude of basal force fluctuations
- We suggest volumetric solid concentration should be incorporated in seismic models as a key parameter describing particle agitation

Abstract

Sediment flows generate ground vibrations by exerting basal force fluctuations on the riverbed, which motivates the use of seismology to indirectly measure flow properties. Linking the force fluctuations and properties of highly concentrated sediment flows, however, remains particularly challenging due to complexities that arise from grain-to-grain interactions. Here we conduct downscaled flume experiments designed to investigate the influence of grain scale processes on the generation of force fluctuations for stratified sediment flows associated with significant grain sorting. We demonstrate that, under such flow conditions, the amplitude of force fluctuations decreases as the volumetric solid concentration increases. We suggest that this dependency reflects the negative relationship between volumetric solid concentration and particle agitation, which in turn controls the amplitude of force fluctuations. We therefore advance that volumetric solid should be incorporated in seismic models as a key parameter describing the particle agitation of highly concentrated sediment flows.

Plain Language Summary

Flowing through the landscape, a wide range of fluvial processes generate high-frequency ground vibrations (> 1 Hz) by exerting force fluctuations on the bed. This evidence has motivated the use of seismology to indirectly measure sediment transport properties, such as the diameter of the transported sediments, the flux, the thickness and velocity of sediment flows. However, it is still particularly challenging to link the force fluctuations and properties of highly concentrated sediment due to complexities that arise from grain scale processes. Here we focus our attention on grain sorting and rheological stratification, which are quite common in such sediment flows but whose effect on force fluctuations has rarely been investigated. To do so we conduct downscaled flume experiments designed to reproduce highly concentrated flows characterized by a wide bimodal grain size distribution typical of mountain streams. We identify the volumetric solid concentration as the key parameter describing the amplitude of basal force fluctuations through its unique link with the flow particle agitation. This finding offers new insights for the interpretation of the force fluctuations generated by highly concentrated flows and underline limits of current theoretical models.

1 Introduction

Flowing through the landscape, rivers generate high-frequency ground vibrations (> 1 Hz) by exerting force fluctuations on their bed (Burtin et al., 2016; Larose et al., 2015). There is well-established evidence that seismic sensors detect ground vibrations from a wide variety of fluvial sediment transport events including very energetic ones (Arattano & Moia, 1999; Burtin et al., 2016; Cook et al., 2018, 2021; Govi et al., 1993; McCoy et al., 2013), calling for seismology as an appealing way to remotely monitor sediment transport characteristics and processes.

Through laboratory experiments and field observations, numerous efforts have recently been dedicated to investigate the relationships between the amplitude of force fluctuations and the properties of various sediment flows, ranging from bedload to debris flows (Allstadt et al., 2020; Bakker et al., 2020; Cole et al., 2009; Coviello et al., 2018, 2019; Gimbert et al., 2019; Haas et al., 2021; Hsu et al., 2014; McCoy et al., 2013; Zhang, Walter, McArdell, Haas, et al., 2021). In parallel, physically-based mechanistic models have been developed to establish quantitative links between flow properties and the seismic signal (Tsai et al., 2012; Gimbert et al., 2019; Bachelet et al., 2021; Farin et al., 2019; Lai et al., 2018; Zhang, Walter, McArdell, Haas, et al., 2021). Models concerning bedload transport predict that sediment flux and transported grain sizes are major control parameters, the former mainly setting the rate of impacts and the latter the impact-released energy. These theoretical expectations have been verified through experiments and field observations under relatively low bedload transport rates (Bakker et al., 2020; Gimbert et al., 2019; Lagarde et al., 2021; Roth et al., 2016).

However, more complexity arises when dealing with highly concentrated sediment flows, for which existing observations reveal not straightforward relationships between flow properties and the amplitude of force fluctuations. Coarse granular and debris flows have been shown to generate stronger force fluctuations compared to finer ones (Haas et al., 2021; Hsu et al., 2014; Zhang, Walter, McArdell, Haas, et al., 2021), but the presence of big particles does not necessarily correspond to high force fluctuations, likely depending on their position relative to the bed (Piantini et al., 2021; Zhang, Walter, McArdell, Haas, et al., 2021). Certain investigations show amplitudes of force fluctuations that are positively correlated with flow thickness and mass (McCoy et al., 2013; Zhang, Walter, McArdell, Haas, et al., 2021), others report poorer correlations when bulk density varies fast (Allstadt et al., 2020), or even negative correlations in the case of mud-saturated debris flows (Hsu et al., 2014). Hsu et al. (2014) illustrate that sediment flow velocity exerts a primary control on force fluctuations, while Allstadt et al. (2020) and Zhang et al. (2021) observe a rather low correlation.

These complex and sometimes contrasting observations suggest the need to investigate more deeply the control of grain scale processes on the generation of force fluctuations (Allstadt et al., 2020). Grain sorting processes (Frey & Church, 2009; Iverson et al., 2010; Johnson et al., 2012) and rheological flow stratification, intended as the occurrence of significant variations of flow rheology over depth (Armanini et al., 2005; GDR MiDi, 2004; Manville & White, 2003; Y. K. Sohn, 1997), may play a role as they influence the distribution of grain sizes and reflect the degree of particle agitation (GDR MiDi, 2004; Iverson et al., 1997; Y. K. Sohn, 1997), respectively. However, these mechanisms have been rarely taken into account for interpreting observations or investigated in experimental works, and are typically neglected in theoretical models (Bachelet et al., 2021; Farin et al., 2019; Lai et al., 2018; Zhang, Walter, McArdell, Haas, et al., 2021). It thus remains unclear to which extent the above-mentioned processes may control the generation of force fluctuations, and whether such control may be described as a function of bulk flow properties.

In order to address this lack, here we conduct downscaled flume experiments designed to reproduce self-triggered highly concentrated flows characterized by a wide bimodal grain size distribution typical of mountain streams, and experiencing significant rheological flow stratification and grain sorting. We investigate their propagation in a steep rough channel while independently measuring flow properties and its seismic signature. We identify the volumetric solid concentration as the key parameter describing the amplitude of basal force fluctuations through its unique link with the flow particle agitation.

2 Methods

2.1 Experimental setup and conditions

We carry out laboratory experiments in a flume composed of a 5-m long and 0.1-m wide straight steep channel (slope of 18%), connected in its upstream part to a 1-m long and on average 0.5-m wide storage area (slope of $0-1\%$) (Figure 1a-b). Every run consists in feeding the upstream storage area with constant liquid discharge Q_l ($Q_l \in [0.48; 0.55\ l/s]$) and sediment flux Q_s ($Q_s \in [70; 100\ g/s]$) whose values are based on similitude criteria to reproduce typical supercritical and fully turbulent flood conditions in mountain rivers (Piantini et al., 2021). We use a bimodal grain size distribution typical of mountain rivers (Casagli et al., 2003; John Wolcott, 1988; Sklar et al., 2017). The sediment size mixture is characterized by two modes corresponding to sand (0.5 mm $< D <$ 2 mm) and cobbles (4 mm $< D <$ 8 mm) (see Figure 4 in (Piantini et al., 2021)), with $D_{50} = 5.16$ mm and $D_{84} = 9$ mm. The bed and side walls of the flume are covered with sediments taken by the same sediment mixture and fixed with silicone. The sediment deposit that forms in the storage area is subject to alternating stages of aggradation and erosion (Figure 1a), with every erosion phases generating sediment pulses that propagate in the downstream steep channel (Figure 1b). Here we investigate specifically sediment pulses. We have investigated 4 sediment pulses in total, two of them are presented in the main text (hereafter referred to as Exp #1 and Exp #2) and the others in the Supporting Information. All the flow properties presented and discussed in the following sections are averaged over these two experiments.

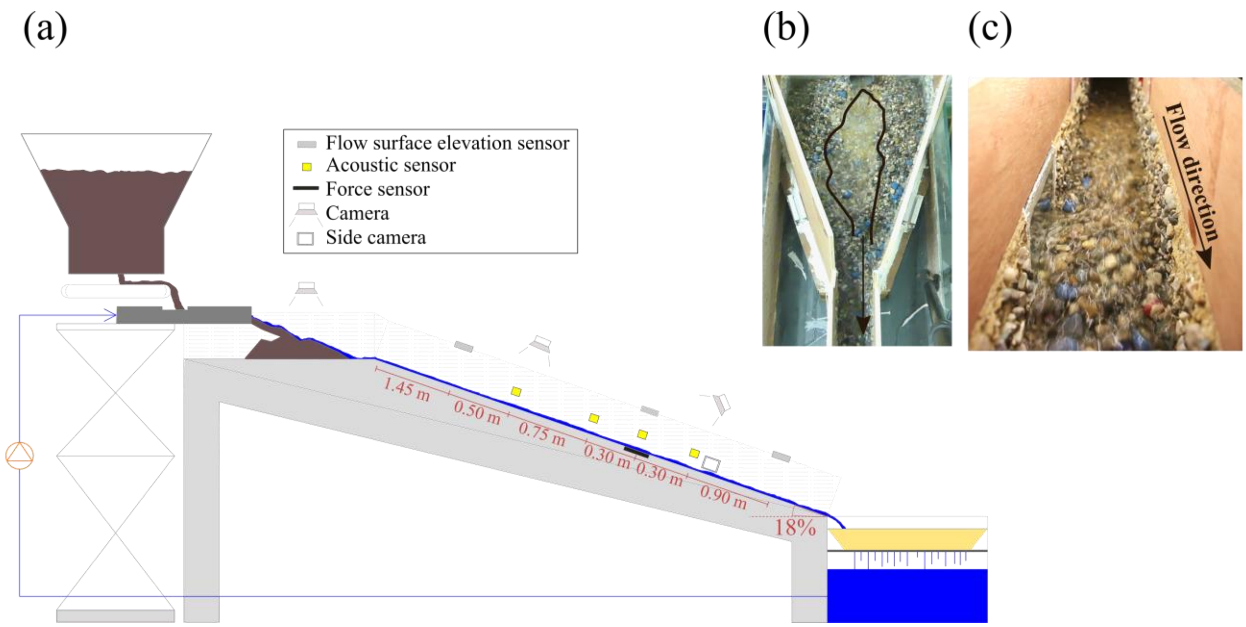

Figure 1. (a) Sketch of the experimental flume. (b) Frame taken from the video recording of the storage area during an experiment. The area interested by the erosion phase is circled in black. (c) Frame taken from the video recording over the force sensor during an experiment.

2.2 Instrumentation

Seismically relevant quantities are measured through seismic and force sensors. Four Glaser-type KRNBB-PC piezoelectric sensors, which we here refer to as seismic sensors, are mounted on the outside of one of the sidewalls of the channel, using mounting brackets and double-sided adhesive tape (Figure 1a and Figure S1). The sensors are connected via an AMP-12BB-J preamplifier to an Elexis Spectrum digitizer with sampling frequency f_s set to 200 kHz. The mean basal force and force fluctuations are measured by coupling a 0.07-m wide and 0.1-m long rectangular steel plate onto the channel bed with two piezoelectric force sensors (model

Kistler Typ 9601A21 connected to a Kistler 5073 charge amplifier) measuring the normal and downslope forces exerted by the flow on the plate (using $f_s = 30$ kHz). The plate is mechanically isolated from the rest of the flume to minimize its sensitivity to flume vibrations, and is covered by sediments fixed with silicone (Supporting Information).

We also monitor several in-stream flow properties simultaneously. We measure the flow surface elevation in three different sections of the channel (Figure 1a) by means of three ultrasonic sensors (Banner Q45UR Series, using $f_s = 100$ Hz). We sample and sieve the sediment flux by hand at the flume outlet with a frequency of about 1 sample / 5 sec. We estimate the volumetric solid concentration by evaluating the bulk density as the ratio between the mean normal stress and the flow surface elevation (Iverson et al., 2010). We also estimate the macroscopic velocity of the sediment flows (U_x) and the downstream velocity of the biggest particles (u_x) by combining multiple sets of observations (Supporting Information). We video record each experiment through a camera (Canon EOS 200D) and a webcam (Microsoft HD LifeCam Cinema) in the upstream and downstream parts of the flume, respectively (Figure 1a). The upstream camera is installed perpendicular to the channel bed and covers a stretch of 0.30 m, while the webcam is inclined to allow a wider look on the channel length (Figure 1c).

2.3 Seismic and force data processing

We analyse the seismic and normal force fluctuation time series through computing the power spectral density (PSD) using Welch's averaging method (Welch, 1967). Time series are split into 50% overlapping segments of 0.5 s for the seismic signal and 1 s for the force signal. Force power and flow property time series are smoothed using a 5-s moving window. We consider the frequency range $100 - 2500$ Hz to avoid dealing with strong plate resonances and the contribution of impacts on the side walls, which are particularly noticeable above 2500 Hz (Figure S2), and to limit the contribution of water flow to the seismic noise (e.g. water pump, water flow in pipes and on the flume), which is significant below 100 Hz (Piantini et al., 2021).

3 Results

3.1 General observations

3.1.1 In-stream transport dynamics

The self-triggered destabilizations of the upstream sediment deposit generate a downstream propagating pulse made of three distinct sediment transport phases exhibiting different dynamics and grain size compositions:

- Phase I ("Front bedload" in Figure 2d, and Figure 2i and Figure 2m) is characterized by a constant and relatively low sediment flux (i.e. similar to that imposed by the boundary conditions to the storage area, $35 < Q_s < 100$ g/s), and a coarse grain size distribution inherited from the coarser surface of the sediment deposit being the first to be destabilized (Piantini et al., 2021). This phase is dilute ($\phi \in [0.15: 0.25]$), exhibits typical bedload dynamics with grains saltating, rolling, and sliding on the bed (see movie

S1 and S2) with a mean downstream particle velocity $u_x \approx 0.27$ m/s (Figure 2e), and lasts for about 60 ± 30 seconds.

- Phase II ("Highly concentrated sediment flow" in Figure 2b-c, and Figure 2i and Figure 2m) is characterized by a high sediment flux ($Q_s > 150$ g/s) exhibiting a wide grain size distribution made of a varying amount of fines ($D < 2$ mm). This phase corresponds to the maximum volume erosion in the sediment deposit causing a thick sediment flow ($\sim 3 - 3.5$ cm) with a downstream propagation that lasts for about 30 ± 10 seconds (Piantini et al., 2021). The flow exhibits a strong vertical rheological stratification (see movie S1 and S2): surface particles are mainly driven by boundary shear stress (i.e. flowing water) and grain collisions, while deeper particles move slower likely as a result of frictional and enduring contacts between grains. A strong increase in fine content during phase II leads to further vertical heterogeneities in terms of grain sizes thanks to the occurrence of grain sorting processes (Frey & Church, 2009; Johnson et al., 2012), for which the biggest particles are pushed towards the surface (see movie S1 and movie S2). When the content of fines is low ($C_{D<2\,mm}^{Phase\ II} < 10$ %), we estimate a mean downstream surface particle velocity of $u_x \approx 0.17$ m/s, while when the content is higher ($C_{D<2\,mm}^{Phase\ II} > 35$ %) we have $u_x \approx 0.39$ m/s (Figure 2e). The average downstream velocity of the thick sediment flow is estimated to be much slower than surface particles ($U_x \approx 0.10$ m/s, Supporting Information). The volumetric solid concentration of phase II is highly variable in time ($\phi \in [0.30{:}\,0.50]$), consistent with previous observations regarding debris flows (Iverson et al., 2010). The observed vertical stratification suggests an increasing volumetric solid concentration with depth, thus ϕ must be seen as depth-averaged. This behaviour appears as similar to observed for sheetflows on steep slopes (Palucis et al., 2018) and highly concentrated sediment flows (Armanini et al., 2005; Manville & White, 2003; Y. K. Sohn, 1997), where a flux of particles driven by shear stress overlays a denser sediment flow that moves *en masse*.

- Phase III %) ("Tail bedload" in Figure 2a, and Figure 2i and Figure 2m) is characterized by a low sediment flux ($35 < Q_s < 150$ g/s) and low values of volumetric solid concentration ($\phi \in [0.15{:}\,0.25]$) similar to phase I. However, it exhibits a wider and finer grain size distribution ($C_{D>8\,mm}^{Phase\ I} = 58\%$ against $C_{D>8\,mm}^{Phase\ III} = 27$. This phase lasts for about 90 ± 15 seconds, and corresponds to the final stage of the erosion processes occurring in the sediment deposit. Phase III is characterized by a typical bedload dynamics (see movie S1 and S2) with a mean downstream particle velocity $u_x \approx 0.30$ m/s.

3.1.2 Force fluctuations and seismic observations

The three phases documented above have distinct seismic and force fluctuation signatures (Figure 2f-g-h and Figure 2j-k-l). Phases I and III generate the highest seismic and force power over the whole frequency range of interest. Phase I is associated with force power on average 3 dB higher than phase III likely as a result of differences in grain size distribution and downstream particle velocity, as expected from existing theories (Farin et al., 2019; Lai et al., 2018; Tsai et al., 2012) and as discussed further in section 4.1. The passage of the highly concentrated sediment flow (phase II, showed between vertical dashed red lines in Figure 2f-i and Figure 2j-m) is materialized by the sharp increase in mean basal force (i.e. sediment flow mass M, Figure 2g and Figure 2k).

Interestingly, it is associated with a strong reduction of on average about 10 dB in both seismic and force power (Figure 2f-g-h and Figure 2j-k-l) compared to phase I and III. We also find that the largest drops in force and seismic power always occur when the maximum flux of fines passes through the sections closest to the respective seismic and force sensors (see yellow squares in Figure 2f-g-h and Figure 2j-k-l). These observations made using the camera are also confirmed by the time delay observed between the lowest levels of force power and the outlet sediment flux measurements characterized by the maximum content of fines, which is consistent with that predicted using the estimated downstream velocity of the sediment flux. In order to better interpret the variations in force power associated with the highly concentrated sediment flow, we push forward our investigation by analysing the link between force power and flow bulk properties.

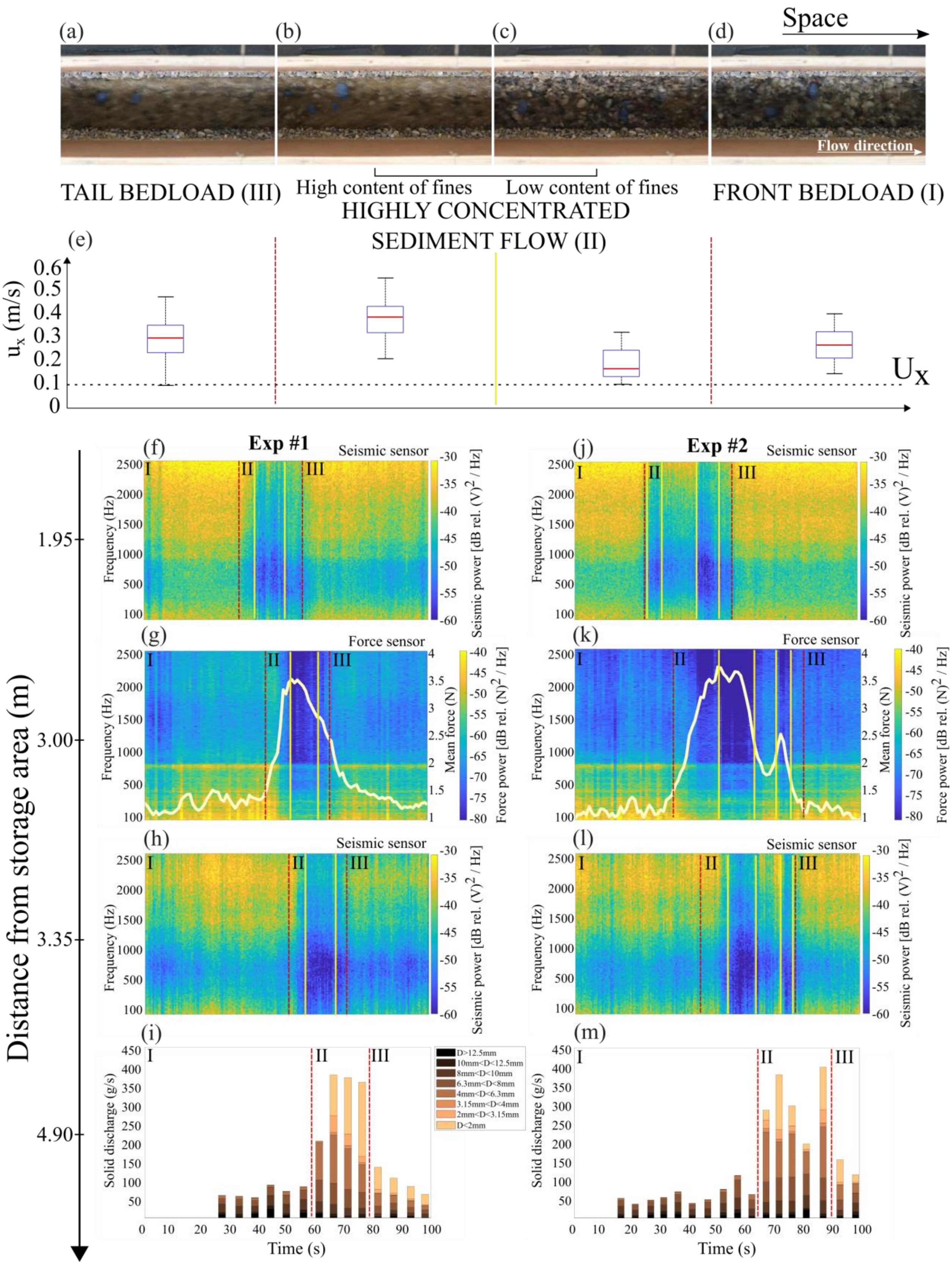
(a)
(b)
(c)
(d)
Space
Flow direction
TAIL BEDLOAD (III)
High content of fines
Low content of fines
HIGHLY CONCENTRATED SEDIMENT FLOW (II)
FRONT BEDLOAD (I)
(e)
u_x (m/s)
U_x
Distance from storage area (m)
1.95
3.00
3.35
4.90
Exp #1
Exp #2
(f)
(g)
(h)
(i)
(j)
(k)
(l)
(m)
Seismic sensor
Force sensor
Frequency (Hz)
Seismic power [dB rel. (V)^2 / Hz]
Force power [dB rel. (N)^2 / Hz]
Mean force (N)
I
II
III
Solid discharge (g/s)
Time (s)
D>12.5mm
10mm<D<12.5mm
8mm<D<10mm
6.3mm<D<8mm
4mm<D<6.3mm
3.15mm<D<4mm
2mm<D<3.15mm
D<2mm

Figure 2. (a-d) Photos from the upstream camera showing the phases of a typical pulse; (e) Box plots for the downstream particle velocity for each phase. The bottom and top of each box are the 25th and 75th percentiles of the sample, while the red line in the middle represents the median. The whiskers above and below each box go to the furthest observations. U_x is shown with the horizontal dotted line. (f-h) and (j-l) Seismic power detected by the upstream and downstream seismic sensor, respectively. It is shown as a function of time and frequency. Different colors refer to different levels of power. (g-k) Force power and mean force detected by the force sensor. (i-m) Outlet sediment flux measurements. Each colored bar refers to the particle diameter displayed in the legend, and the bar length is proportional to the percentage in weight of the related size. The vertical dashed red lines divide the three different phases presented in the photos above, while the yellow squares delimit the time interval with the maximum content of fines in phase II.

3.2 Linking force power with the properties of the highly concentrated sediment flows

In Figure 3 we express flow surface elevation (h), mean basal force ($\bar{F}$), and volumetric solid concentration (Φ) as a function of the measured force power. The very first seconds of the highly concentrated sediment flows are characterized by weak positive relationships between force power and h, $\bar{F}$, and Φ (Figure 3b-d and Figure 3f-h). However, at this stage of the experiment these measurements are quite uncertain as a result of being affected by local and transient grain depositions (Supporting Information). Past an inflexion point corresponding to $\Phi = 0.36$ for Exp #1 and $\Phi = 0.21$ for Exp #2, the relationship between force power and flow properties becomes negative. We observe large counter-clockwise hysteresis in the relationships between force power and h and $\bar{F}$: a given mean basal force and flow surface elevation is associated with significantly different values of force power (5 up to 10 dB differences). This hysteresis behaviour is due to force power decreasing and remaining low after peak h and $\bar{F}$ are reached (Figure 2f and Figure 2j, and Figure 3a and Figure 3e). Interestingly, this hysteresis is no longer significantly observed when force power is evaluated versus Φ (Figure 3d and Figure 3h), in which case maximum Φ always corresponds to minimum force power (Figure 3b and Figure 3f). Although a small clockwise hysteresis may be distinguished between force power and Φ for the presently considered examples, we do not consider it as significant because (i) it is not systematically observed for other sediment flows presented in the Supporting Information, where the rising and falling limbs of Φ collapse on a unique curve, and (ii) it becomes much less clear when reducing the moving average window size applied for smoothing the data, as opposed to versus h and $\bar{F}$ (Supporting Information). Our finding of a direct link between force power and Φ is also supported by observations at shorter time scales. Indeed, we observe drastic changes in the relationship between force power and h and $\bar{F}$, materialized by a small loop around $t = 35$ s in Exp #2 (Figure 3f-g) that are no longer visible in Figure 3h as a result of being associated with according changes in Φ.

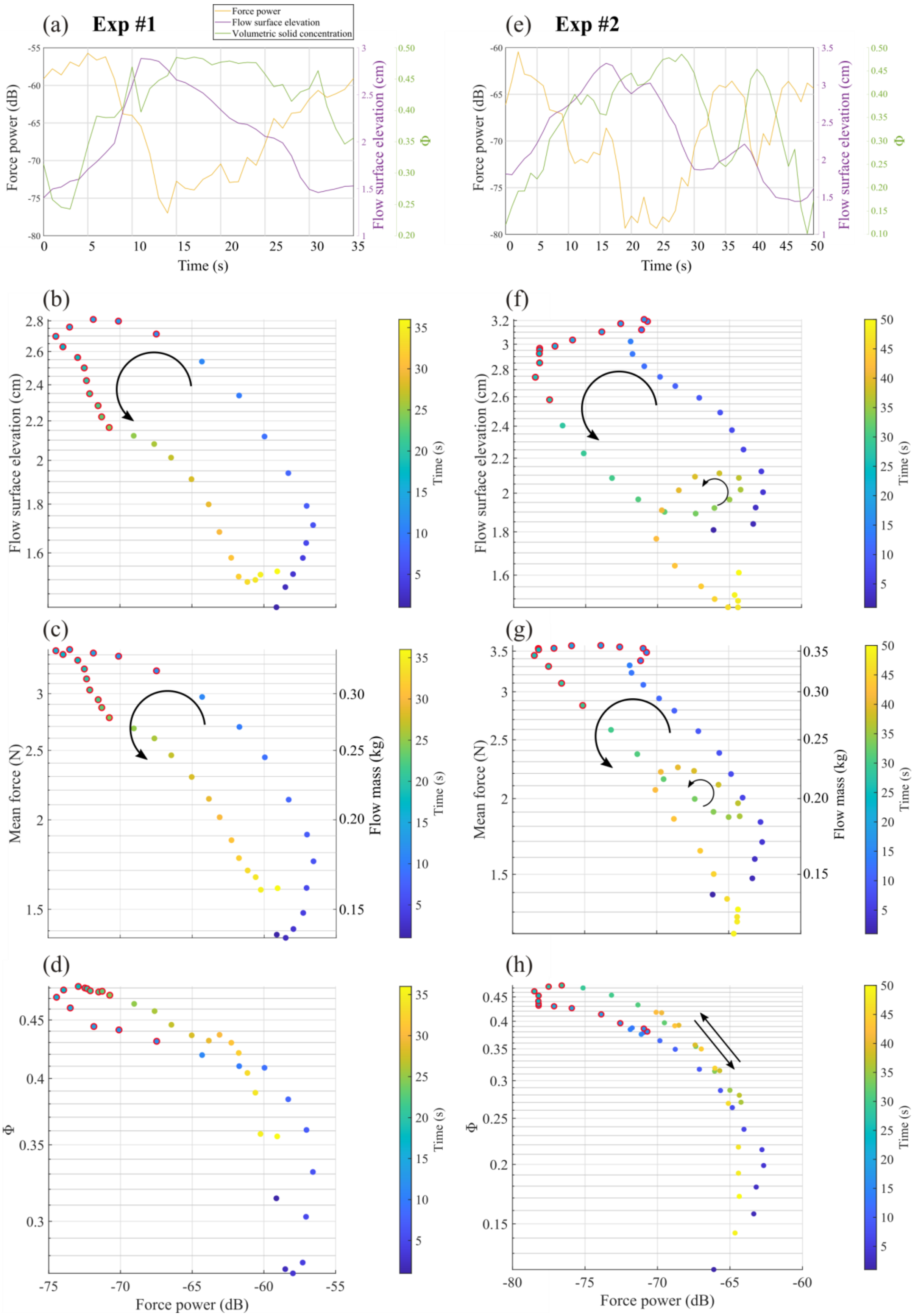
(a) Exp #1
Force power
Flow surface elevation
Volumetric solid concentration
Force power (dB)
Flow surface elevation (cm)
Φ
Time (s)
(b)
(c)
(d)
Mean force (N)
Flow mass (kg)
Force power (dB)
(e) Exp #2
(f)
(g)
(h)

Figure 3. All panels refer to phase II. (a) and (e) show the evolution in time of the force power, h, and Φ. The log-log scatterplots of (b-c-d) and (f-g-h) show force power on the x axis and flow properties on the y axis. M is computed by multiplying the mean force by g. The time interval when the content of fines is maximum is marked in the scatterplots with red circles.

4 Discussion

4.1 Do existing theories explain our observations?

We find that the front bedload (phase I) is characterized by a slightly higher level of force power ($+3$ dB) than that of the tail bedload (phase III), both of which generate significantly higher force power levels ($+10$ dB) than that of the highly concentrated sediment flow (phase II). Sediment transport dynamics in phase I and III appears to be most consistent with that described in previous theories (Farin et al., 2019; Lai et al., 2018; Tsai et al., 2012), where force power is generated by the sum of individual particles impacting the bed at a rate and with a force that is mostly set by (i) the average downstream grain velocity, (ii) the grain size and (iii) the bed roughness. Particles constituting the front bedload move slower than those of the tail bedload ($u_x = 0.27$ m/s against $u_x = 0.30$ m/s), are associated with similar fluxes, but are on average coarser as the percentage of particles > 8 mm is double ($C_{D>8\ mm}^{Phase\ I} = 58\%$ and $C_{D>8\ mm}^{Phase\ III} = 27\%$). As a consequence, slightly larger grains likely explain the slightly higher force power of phase I, especially given the expected prevalence control of the larger grain fraction for our grain size distribution (Supporting Information).

Sediment transport dynamics as formulated in existing theories however cannot explain the force power associated with the highly concentrated sediment flow (phase II, Figure 3a and Figure 3c). During this phase, force power decreases abruptly by about -10 dB in less than 5 seconds (Figure 3a and Figure 3c). Such a reduction is not associated with a decrease in sediment flux, which in fact increases, nor in a decrease of grain size, as the coarse fraction of the highly concentrated sediment is almost constant ($C_{D>8\ mm}^{Phase\ II} = 8\% \pm 2$ for Exp #1 and $C_{D>8\ mm}^{Phase\ II} = 14\% \pm 2$ for Exp #2). We also exclude strong decreases in the averaged sediment flow velocity as a potential origin of this behaviour, since we do not observe spatial disconnections within phase II. As presented in section 3.1, particles at the surface are more agitated and move faster than underlying sediments. This is particularly evident when grain sorting occurs. Another possibility could be that these particles constitute the main source of force fluctuations as a result of being the biggest and the fastest, and that the thicker sediment flow beneath them dampens their contribution, resulting in lower force fluctuations on the bed as observed in the presence of static sediment deposits (Kean et al., 2015; McCoy et al., 2013). However, we do not find this process primarily explains our observations because: (i) when particles at the surface reach maximum velocity, force power in fact reaches its minimum (phase II with the presence of fines, Figure 2e) and (ii) there is not a unique link but a hysteresis between force power and the thickness of the sediment flow (see hysteresis in Figure 3b and Figure 3f) as one would expect if this latter controlled the attenuation of force fluctuations.

4.2 Volumetric solid concentration helps deciphering the force fluctuations generated by the highly concentrated sediment flows

The key observation yielding further insight into the underlying source of reduced force fluctuations of the highly concentrated sediment flow (phase II) is the negative relationship and suppressed hysteresis behaviour between force power and volumetric solid concentration (Figure 3b and Figure 3f). Volumetric solid concentration is known to be a proxy for particle agitation for dense granular flows, commonly described as granular temperature (Armanini et al., 2005; Campbell, 1990; GDR MiDi, 2004; Iverson et al., 1997). Rapid and agitated granular flows are characterized by low values of Φ as they dilate, while less agitated flows mean that particles have poor capability to move past one other and tend to jam with slow long-lasting contacts, leading to an increase in solid concentration (da Cruz et al., 2005; Forterre & Pouliquen, 2008). Since particle agitation controls inter-particle collisions and impacts to the bed (Bachelet et al., 2021; Farin et al., 2019), high values of solid concentration are associated with low force fluctuations. The evolution of Φ over time may also explain the observed (i) presence of the hysteresis and (ii) negative relationships between h and M and force power. Hysteresis may be due to the percolation of fines in the voids within the coarse fraction of the mixture, which optimizes the space occupied by particles and allows for an increase in Φ and thus a decrease in the amplitude of force fluctuations regardless of h or M. Fines thus help dampening force fluctuations primarily through increasing the Φ rather than pushing big particles far from the bed, although this latter mechanism may still occur at a secondary level.

The finding of a negative relationship between force power and Φ is consistent with the results of Allstadt et al. (2020), who highlight the existence of a negative correlation between the normal fluctuating stresses and the bulk density of experimental debris flows. This finding could appear in contradiction with Coviello et al. (2018) who show that a hyperconcentrated flow generates higher seismic signals than more dilute sediment transport, however in their case the coarse grain fraction also increase dramatically with sediment concentration. Past observations of positive correlation in the relationships between h and M and force power as opposed to this study (Allstadt et al., 2020; McCoy et al., 2013; Zhang, Walter, McArdell, Haas, et al., 2021) could also be explained in terms of Φ. Indeed, in the debris flows investigated by Allstadt et al. (2020) and Zhang et al. (2021), bulk density decreases as h and M increase. Our interpretation may be also consistent with the experiments of Hsu et al. (2014), who argue that the slightly negative correlation observed between the force fluctuations and mean force for “the least collisional” mud-saturated granular flow could be explained by a high ratio of solid to fluid volume fraction. We therefore suggest that a positive relationship between force power and flow surface elevation holds only when the latter is the result of dilation of the flow, causing enhanced particle agitation. We acknowledge that this is often the case for natural debris flows (Iverson, 1997), although the extent it would apply to other sediment flows such as sheetflows or highly concentrated sediment flows remains uncertain. Nevertheless, our present finding may provide a path to unify these various flows into a single framework, in which the key requirement would be to properly describe the dependency of volumetric solid concentration on flow characteristics.

4.3 Implications for theoretical models

Particle agitation controls the rate of impacts and impact velocities of particles of sediment flows. In existing theoretical models, it is assumed to be a function of the average downstream velocity of the flow (Bachelet et al., 2021; Farin et al., 2019; Zhang, Walter, McArdell, Haas, et al., 2021), while volumetric solid concentration only comes into play through controlling the number of particles impacting the bed (Farin et al., 2019; Zhang, Walter, McArdell, Haas, et al., 2021). Here we propose that particle agitation should be incorporated as a function of volumetric solid concentration or bulk density, equivalently (Jenkins & Askari, 1999). This would cause the link between force fluctuations and volumetric solid concentration to be negative rather than positive, at least for sufficiently highly concentrated sediment flows.

5 Conclusions

We carry out laboratory experiments to explore the influence of grain scale processes in the generation of force fluctuations of highly concentrated sediment flows. The key observation yielding further insight onto the underlying source of force fluctuations is the clear negative relationship between their amplitude and volumetric solid concentration. We interpret this result by considering the volumetric solid concentration as a proxy for the degree of particle agitation. Our present finding may also provide a path to unify various flows into a single framework, in which the key requirement would be to properly describe the dependency of volumetric solid concentration on flow characteristics.

Acknowledgments

The authors declare no conflict of interest. This research has been supported by the Agence Nationale de la Recherche (grant no. 17-CE01-0008). We acknowledge the support of the INRAE Research Centre of Grenoble for the laboratory and instrumental equipment. We thank Jeroni Salens for helping in the development of the force plate and sensor, and Zavier Berti for the fruitful scientific discussions.

Open Research

The data analysed during the current study are available on the Zenodo platform via

https://doi.org/10.5281/zenodo.6761000

References

Allstadt, K. E., Farin, M., Iverson, R. M., Obryk, M. K., Kean, J. W., Tsai, V. C., Rapstine, T. D., & Logan, M. (2020). Measuring Basal Force Fluctuations of Debris Flows Using Seismic Recordings and Empirical Green's Functions. *Journal of Geophysical Research: Earth Surface*, *125*(9). https://doi.org/10.1029/2020JF005590

Arattano, M., & Moia, F. (1999). Monitoring the propagation of a debris flow along a torrent. *Hydrological Sciences Journal*, *44*(5), 811–823. https://doi.org/10.1080/02626669909492275

Armanini, A., Capart, H., Fraccarollo, L., & Larcher, M. (2005). Rheological stratification in experimental free-surface flows of granular–liquid mixtures. *Journal of Fluid Mechanics*, *532*, 269–319. https://doi.org/10.1017/S0022112005004283

Bachelet, V., Mangeney, A., Toussaint, R., DeRosny, J., Farin, M., & Hibert, C. (2021). *Acoustic emissions of nearly steady and uniform granular flows: A proxy for flow dynamics and velocity fluctuations*. https://doi.org/10.48550/ARXIV.2101.04161

Bakker, M., Gimbert, F., Geay, T., Misset, C., Zanker, S., & Recking, A. (2020). Field Application and Validation of a Seismic Bedload Transport Model. *Journal of Geophysical Research: Earth Surface*, *125*(5). https://doi.org/10.1029/2019JF005416

Burtin, A., Hovius, N., & Turowski, J. M. (2016). Seismic monitoring of torrential and fluvial processes. *Earth Surface Dynamics*, *4*(2), 285–307. https://doi.org/10.5194/esurf-4-285-2016

Campbell, C. S. (1990). *Rapid Granular Flows*. 36.

Casagli, N., Ermini, L., & Rosati, G. (2003). Determining grain size distribution of the material composing landslide dams in the Northern Apennines: Sampling and processing methods. *Engineering Geology*, *69*(1–2), 83–97. https://doi.org/10.1016/S0013-7952(02)00249-1

Cole, S. E., Cronin, S. J., Sherburn, S., & Manville, V. (2009). Seismic signals of snow-slurry lahars in motion: 25 September 2007, Mt Ruapehu, New Zealand. *Geophysical Research Letters*, *36*(9), L09405. https://doi.org/10.1029/2009GL038030

Cook, K. L., Andermann, C., Gimbert, F., Adhikari, B. R., & Hovius, N. (2018). Glacial lake outburst floods as drivers of fluvial erosion in the Himalaya. *Science*, *362*(6410), 53–57. https://doi.org/10.1126/science.aat4981

Cook, K. L., Rekapalli, R., Dietze, M., Pilz, M., Cesca, S., Rao, N. P., Srinagesh, D., Paul, H., Metz, M., Mandal, P., Suresh, G., Cotton, F., Tiwari, V. M., & Hovius, N. (2021). Detection and potential early warning of catastrophic flow events with regional seismic networks. *Science*, *374*(6563), 87–92. https://doi.org/10.1126/science.abj1227

Coviello, V., Arattano, M., Comiti, F., Macconi, P., & Marchi, L. (2019). Seismic Characterization of Debris Flows: Insights into Energy Radiation and Implications for Warning. *Journal of Geophysical Research: Earth Surface*, *124*(6), 1440–1463. https://doi.org/10.1029/2018JF004683

Coviello, V., Capra, L., Vázquez, R., & Márquez-Ramírez, V. H. (2018). Seismic characterization of hyperconcentrated flows in a volcanic environment: Seismic characterization of hyperconcentrated flows. *Earth Surface Processes and Landforms*, *43*(10), 2219–2231. https://doi.org/10.1002/esp.4387 da Cruz, F., Emam, S., Prochnow, M., Roux, J.-N., & Chevoir, F. (2005). Rheophysics of dense granular materials: Discrete simulation of plane shear flows. *Physical Review E*, *72*(2), 021309. https://doi.org/10.1103/PhysRevE.72.021309

Farin, M., Tsai, V. C., Lamb, M. P., & Allstadt, K. E. (2019). A physical model of the high-frequency seismic signal generated by debris flows. *Earth Surface Processes and Landforms*, *44*(13), 2529–2543. https://doi.org/10.1002/esp.4677

Forterre, Y., & Pouliquen, O. (2008). Flows of Dense Granular Media. *Annual Review of Fluid Mechanics*, *40*(1), 1–24. https://doi.org/10.1146/annurev.fluid.40.111406.102142

Frey, P., & Church, M. (2009). How River Beds Move. *Science*, *325*(5947), 1509–1510. https://doi.org/10.1126/science.1178516

GDR MiDi. (2004). On dense granular flows. *The European Physical Journal E*, *14*(4), 341–365. https://doi.org/10.1140/epje/i2003-10153-0

Gimbert, F., Fuller, B. M., Lamb, M. P., Tsai, V. C., & Johnson, J. P. L. (2019). Particle transport mechanics and induced seismic noise in steep flume experiments with accelerometer-embedded tracers: Experimental Testing of Seismic Noise Generated by Sediment Transport. *Earth Surface Processes and Landforms*, *44*(1), 219–241. https://doi.org/10.1002/esp.4495

Govi, M., Maraga, F., & Moia, F. (1993). Seismic detectors for continuous bed load monitoring in a gravel stream. *Hydrological Sciences Journal*, *38*(2), 123–132. https://doi.org/10.1080/02626669309492650

Haas, T., Åberg, A. S., Walter, F., & Zhang, Z. (2021). Deciphering seismic and normal-force fluctuation signatures of debris flows: An experimental assessment of effects of flow composition and dynamics. *Earth Surface Processes and Landforms*, esp.5168. https://doi.org/10.1002/esp.5168

Hsu, L., Dietrich, W. E., & Sklar, L. S. (2014). Mean and fluctuating basal forces generated by granular flows: Laboratory observations in a large vertically rotating drum. *Journal of Geophysical Research: Earth Surface*, *119*(6), 1283–1309. https://doi.org/10.1002/2013JF003078

Iverson, R. M. (1997). The physics of debris flows. *Reviews of Geophysics*, *35*(3), 245–296. https://doi.org/10.1029/97RG00426

Iverson, R. M., Logan, M., LaHusen, R. G., & Berti, M. (2010). The perfect debris flow? Aggregated results from 28 large-scale experiments. *Journal of Geophysical Research*, *115*(F3), F03005. https://doi.org/10.1029/2009JF001514

Iverson, R. M., Reid, M. E., & LaHusen, R. G. (1997). Debris-flow mobilization from landslides. *Annual Review of Earth and Planetary Sciences*, *25*(1), 85–138. https://doi.org/10.1146/annurev.earth.25.1.85

Jenkins, J. T., & Askari, E. (1999). *Hydraulic theory for a debris flow supported on a collisional shear layer*. *9*(3), 6.

John Wolcott. (1988). Nonfluvial Control of Bimodal Grain-Size Distributions in River-Bed Gravels. *SEPM Journal of Sedimentary Research*, *Vol. 58*. https://doi.org/10.1306/212F8ED6-2B24-11D7-8648000102C1865D

Johnson, C. G., Kokelaar, B. P., Iverson, R. M., Logan, M., LaHusen, R. G., & Gray, J. M. N. T. (2012). Grain-size segregation and levee formation in geophysical mass flows: LEVEE FORMATION IN GEOPHYSICAL FLOWS. *Journal of Geophysical Research: Earth Surface*, *117*(F1), n/a-n/a. https://doi.org/10.1029/2011JF002185

Kean, J. W., Coe, J. A., Coviello, V., Smith, J. B., McCoy, S. W., & Arattano, M. (2015). Estimating rates of debris flow entrainment from ground vibrations: GROUND VIBRATIONS FROM DEBRIS FLOWS. *Geophysical Research Letters*, *42*(15), 6365–6372. https://doi.org/10.1002/2015GL064811

Lagarde, S., Dietze, M., Gimbert, F., Laronne, J. B., Turowski, J. M., & Halfi, E. (2021). Grain-Size Distribution and Propagation Effects on Seismic Signals Generated by Bedload Transport. *Water Resources Research*, *57*(4). https://doi.org/10.1029/2020WR028700

Lai, V. H., Tsai, V. C., Lamb, M. P., Ulizio, T. P., & Beer, A. R. (2018). The Seismic Signature of Debris Flows: Flow Mechanics and Early Warning at Montecito, California. *Geophysical Research Letters*, *45*(11), 5528–5535. https://doi.org/10.1029/2018GL077683

Larose, E., Carrière, S., Voisin, C., Bottelin, P., Baillet, L., Guéguen, P., Walter, F., Jongmans, D., Guillier, B., Garambois, S., Gimbert, F., & Massey, C. (2015). Environmental seismology: What can we learn on earth surface processes with ambient noise? *Journal of Applied Geophysics*, *116*, 62–74. https://doi.org/10.1016/j.jappgeo.2015.02.001

Manville, V., & White, J. D. L. (2003). Incipient granular mass flows at the base of sediment-laden floods, and the roles of flow competence and flow capacity in the deposition of stratified bouldery sands. *Sedimentary Geology*, *155*(1–2), 157–173. https://doi.org/10.1016/S0037-0738(02)00294-4

McCoy, S. W., Tucker, G. E., Kean, J. W., & Coe, J. A. (2013). Field measurement of basal forces generated by erosive debris flows: DEBRIS FLOW BASAL FORCE. *Journal of Geophysical Research: Earth Surface*, *118*(2), 589–602. https://doi.org/10.1002/jgrf.20041

Palucis, M. C., Ulizio, T., Fuller, B., & Lamb, M. P. (2018). Intense Granular Sheetflow in Steep Streams. *Geophysical Research Letters*, *45*(11), 5509–5517. https://doi.org/10.1029/2018GL077526

Piantini, M., Gimbert, F., Bellot, H., & Recking, A. (2021). Triggering and propagation of exogenous sediment pulses in mountain channels: Insights from flume experiments with seismic monitoring. *Earth Surface Dynamics*, *9*(6), 1423–1439. https://doi.org/10.5194/esurf-9-1423-2021

Roth, D. L., Brodsky, E. E., Finnegan, N. J., Rickenmann, Dieter., Turowski, J. M., & Badoux, A. (2016). Bed load sediment transport inferred from seismic signals near a river. *Journal of Geophysical Research: Earth Surface*, *121*(4), 725–747. https://doi.org/10.1002/2015JF003782

Sklar, L. S., Riebe, C. S., Marshall, J. A., Genetti, J., Leclere, S., Lukens, C. L., & Merces, V. (2017). The problem of predicting the size distribution of sediment supplied by hillslopes to rivers. *Geomorphology*, *277*, 31–49. https://doi.org/10.1016/j.geomorph.2016.05.005

Tsai, V. C., Minchew, B., Lamb, M. P., & Ampuero, J.-P. (2012). A physical model for seismic noise generation from sediment transport in rivers: SEISMIC NOISE FROM SEDIMENT TRANSPORT. *Geophysical Research Letters*, *39*(2), n/a-n/a. https://doi.org/10.1029/2011GL050255

Welch, P. (1967). The use of fast Fourier transform for the estimation of power spectra: A method based on time averaging over short, modified periodograms. *IEEE Transactions on Audio and Electroacoustics*, *15*(2), 70–73. https://doi.org/10.1109/TAU.1967.1161901

Y. K. Sohn. (1997). On Traction-Carpet Sedimentation. *SEPM Journal of Sedimentary Research*, *Vol. 67*. https://doi.org/10.1306/D42685AE-2B26-11D7-8648000102C1865D

Zhang, Z., Walter, F., McArdell, B. W., Haas, T., Wenner, M., Chmiel, M., & He, S. (2021). Analyzing Bulk Flow Characteristics of Debris Flows Using Their High Frequency Seismic Signature. *Journal of Geophysical Research: Solid Earth*, *126*(12). https://doi.org/10.1029/2021JB022755

Zhang, Z., Walter, F., McArdell, B. W., Wenner, M., Chmiel, M., de Haas, T., & He, S. (2021). Insights From the Particle Impact Model Into the High-Frequency Seismic Signature of Debris Flows. *Geophysical Research Letters*, *48*(1). https://doi.org/10.1029/2020GL088994

Geophysical Research Letters

Supporting Information for

Volumetric solid concentration as a main proxy for basal force fluctuations generated by highly concentrated sediment flows

Marco Piantini[1,2], Florent Gimbert[1], Evangelos Korkolis[1], Romain Rousseau[2], Hervé Bellot[2], and Alain Recking[2]

[1]University Grenoble Alpes, CNRS, IRD, Institute for Geosciences and Environmental Research (IGE), Grenoble, France

[2] University Grenoble Alpes, INRAE, ETNA, Grenoble, France

Contents of this file

Text S1 to S7
Figures S1 to S6

Additional Supporting Information (Files uploaded separately)

Captions for Movies S1 to S2

Introduction

In text S1 we give supplementary information about the installation of the piezoelectric sensors and the installation and calibration of the force plate and sensor. In text S2 we provide specific information on how we estimate the volumetric solid concentration and the downstream particle and sediment flow velocity. In text S3 we show the results of a supplementary experiment carried out to investigate the seismic signature of different particle impacts on the flume. In text S4 we show the uncertainties in flow properties measurements at the beginning of the highly concentrated sediment flow. In text S5 we show other experiments not presented in the main manuscript. In text S6 we show the control of the coarse fraction of the sediment mixture on force fluctuations through applying a simplified framework from the model of Tsai et al. (2021). Finally, in text S7, we show the relationships between flow properties and force power by changing the moving average window size for the experiments presented in the main manuscript.

Text S1. Installation of the piezoelectric sensors and force plate and sensor

The piezoelectric sensors are mounted on the outside of one of the sidewalls of the channel, using mounting brackets and double-sided adhesive tape (Figure S1a). The force plate and force sensor have been installed to maximize its isolation from external flume vibrations. The force plate is supported by the two force sensors (Figure S1b), which in turn rest on a steel support piece that is mechanically connected to the channel substructure (Figure S1a and Figure S1b). The stiffness of the support piece is high enough to consider that all impacts on the force plate are totally transmitted to the force sensors. As the flume rests on a substructure, shock absorbers are placed between the flume and the substructure to avoid the transmission of vibration to the force sensors from the substructure (Figure S1c). The force plate and the rest of the flume bed are connected by 5 mm-long seals (Figure S1d). To ensure continuity with the channel bed roughness, we cover with silicone and sediments the seals and the force plate like the rest of the channel bed (Figure S1e). The force sensors have been fitted under a preload of 25 kHz to ensure measurements stability and linearity between the applied load and the sensor output.

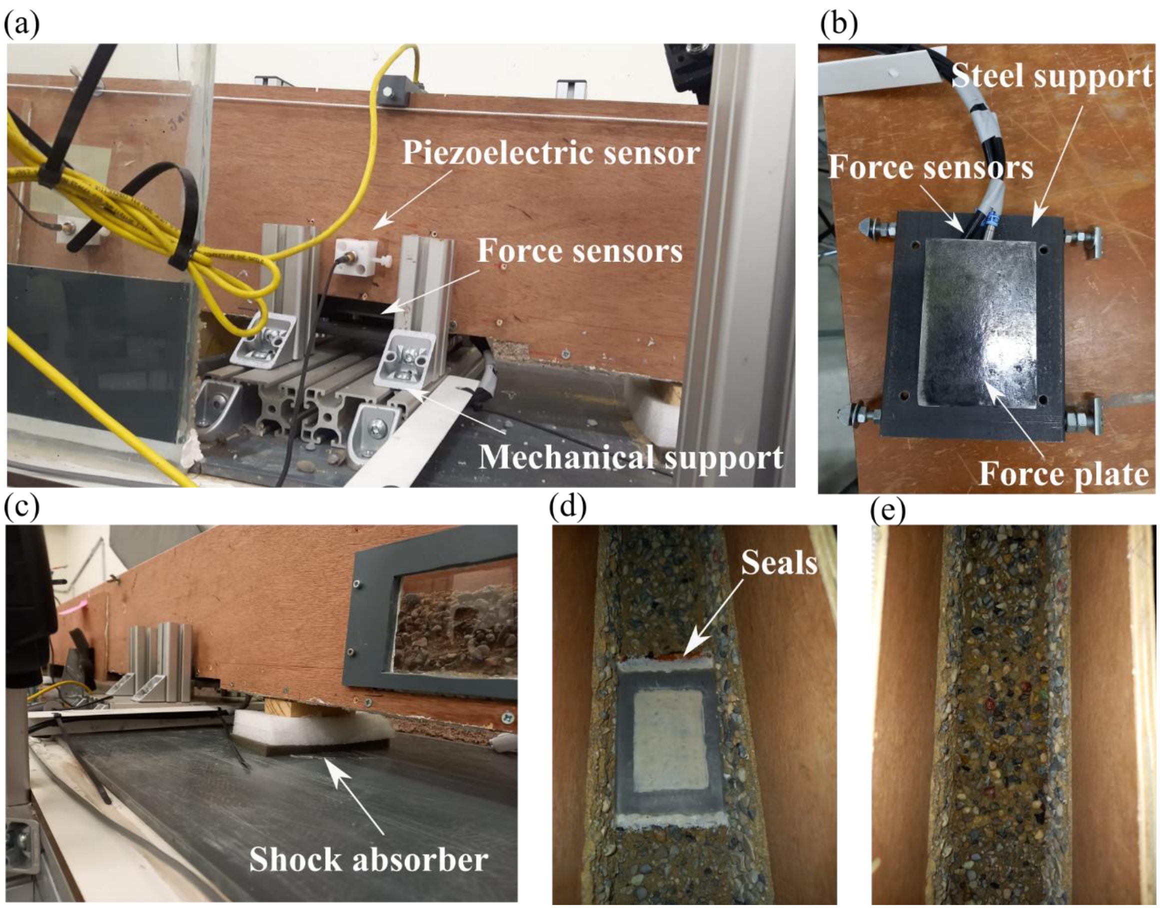

Figure S1. (a-e) Photos of the experimental setup and instruments. (a) Side view of the piezoelectric sensor mounted on the flume sidewall. Below are the different parts installed for the force measurements, i.e. the force sensors and their supports. (b) Photo of the force sensors, force plate, and steel support before installation. (c) Side view of the flume with shock absorbers between the channel bed and substructure. (d) Top view over the force plate. Lateral seals are visible. (e) Top view over the force plate after adding silicone and sediments.

Text S2. Estimations of volumetric solid concentration and particle and sediment flow velocity

We estimate the bulk density of the sediment flows following Iverson et al. (2010):

$$\rho(t) \approx \frac{\sigma_{bed}(t)}{gh(t)cos\theta} \tag{1}$$

where σ_{bed} is the mean basal normal stress, i.e. the mean basal normal force divided by the area of the force plate, g is acceleration due to gravity, $h(t)$ is the flow surface elevation, and θ is the channel slope. We assume that the mean basal normal stress balances the slope-normal static weight of the flow, which is totally supported by the force plate. From the bulk density estimation, the volumetric solid concentration can be computed as follow:

$$\phi(t) = 1 - \frac{\rho_{water}}{\rho(t)} \tag{2}$$

We estimate the macroscopic velocity of the highly concentrated sediment flow (U_x) in three different ways: (i) by tracking the flow through the cameras installed along the channel; (ii) by evaluating time delays in the surface flow elevation measurements; (iii) by evaluating time delays in the seismic measurements. If one of the three estimations differ from the others by $\pm 50\%$, we consider it incorrect and we compute the average of the remaining ones. We also estimate the local downstream velocity of individual particles in the upper part of the flow (u_x) by manually tracking their displacement between consecutive frames taken by the upstream camera. We consider the biggest particles of the sediment mixture for practical reasons, as they are coloured in blue and therefore easy to identify, and because they play a major role in generating seismic vibrations through highly energetic impacts (Tsai et al., 2012).

Text S3. The sensitivity of the piezoelectric sensors to particle impacts

We carry out specific experiments to investigate the sensitivity of the piezoelectric sensors to different mechanisms potentially generating flume vibrations such as particle impacts on the bed and on the sidewalls. To do so we drop a pebble of known mass ($m = 6.6$ g) from a fixed height ($z = 5$ cm) and we use a hand-made pendulum that allows for the same force impact on the sidewall where the sensor is installed. We produce three identical impacts at the same section and then we compute the power spectral density with the Welch's method. In Figure S2 we show the seismic power of the average over the three impacts. We observe that impacts on the sidewall dominate over impacts on the bed in the whole frequency range, but this difference is significant especially at high frequency (over 2500 Hz).

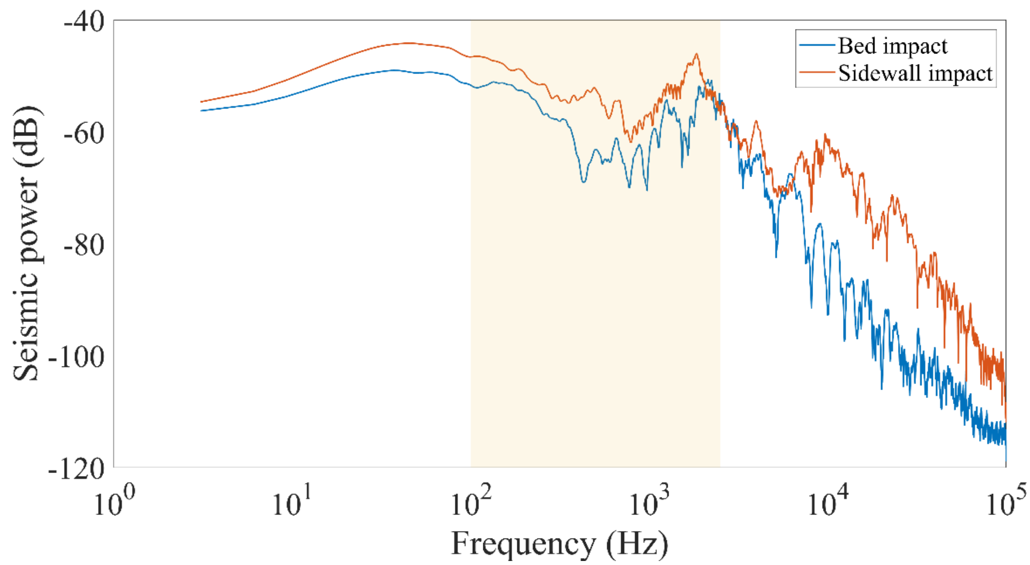

Figure S2. Seismic power as a function of frequency for the impact to the bed (blue curve) and to the sidewall (orange curve). The brownish area shows the frequency range chosen for the analysis.

Text S4. Uncertainties in flow properties measurements at the beginning of the highly concentrated sediment flow

The very first seconds of phase II are characterized by a different relationship between the investigated flow properties and force power compared to the rest of the highly concentrated sediment flow (Figure 3b-c-d and Figure 3f-g-h). A similar behaviour was observed by Allstadt et al. (2020), who pointed out that the unsaturated flow front showed a different link with basal force fluctuations compared to denser parts of the debris flow. It may indicate that below a certain value, an increased bulk density coincides with higher particle impact rate to the bed, leading to stronger force fluctuations as hypothesized by existing theoretical models (Farin et al., 2019; Tsai et al., 2012). However, we must acknowledge that in our setup there exist uncertainties on flow properties computations within this early stage of phase II. Indeed, the video recordings reveal that sometimes clusters of sediments get stuck along the channel (as presented by Piantini et al. (2021)) just before the development and passage of the denser flow.

When occurring above the force plate, these temporal depositions affect the measurements, leading to incorrect conclusions since they do not reflect the dynamics of phase II.

Text S5. Additional experiments

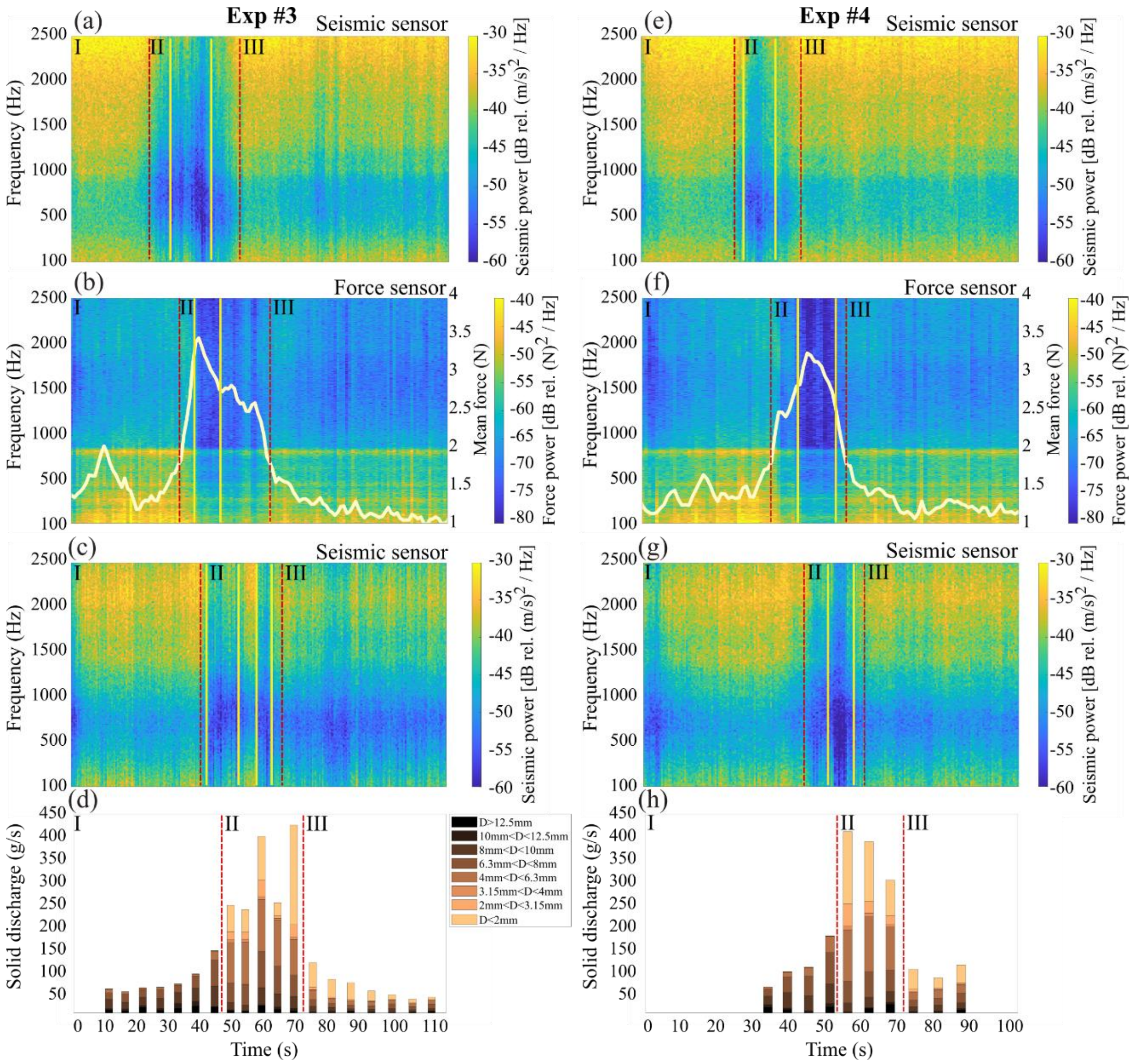

Figure S3. (a-c) and (e-g) Seismic power detected by the upstream and downstream seismic sensor, respectively. It is shown as a function of time and frequency; different colours refer to different levels of power. (b-f) Force power detected by the force sensor. We note that a band of resonance is visible around 1000 Hz. (d-h) Outlet sediment flux measurements. Each coloured bar refers to the particle diameter displayed in the legend, while the bar length is proportional to the percentage in weight of the related size. It's worth recalling that the absence of sediment flux measurements does not necessarily correspond to zero sediment flux, as measurements are by hand and not continuous in time. The vertical dashed red lines divide the three different phases, while the yellow squares delimit the time interval with the maximum content of fine sediments in phase II.

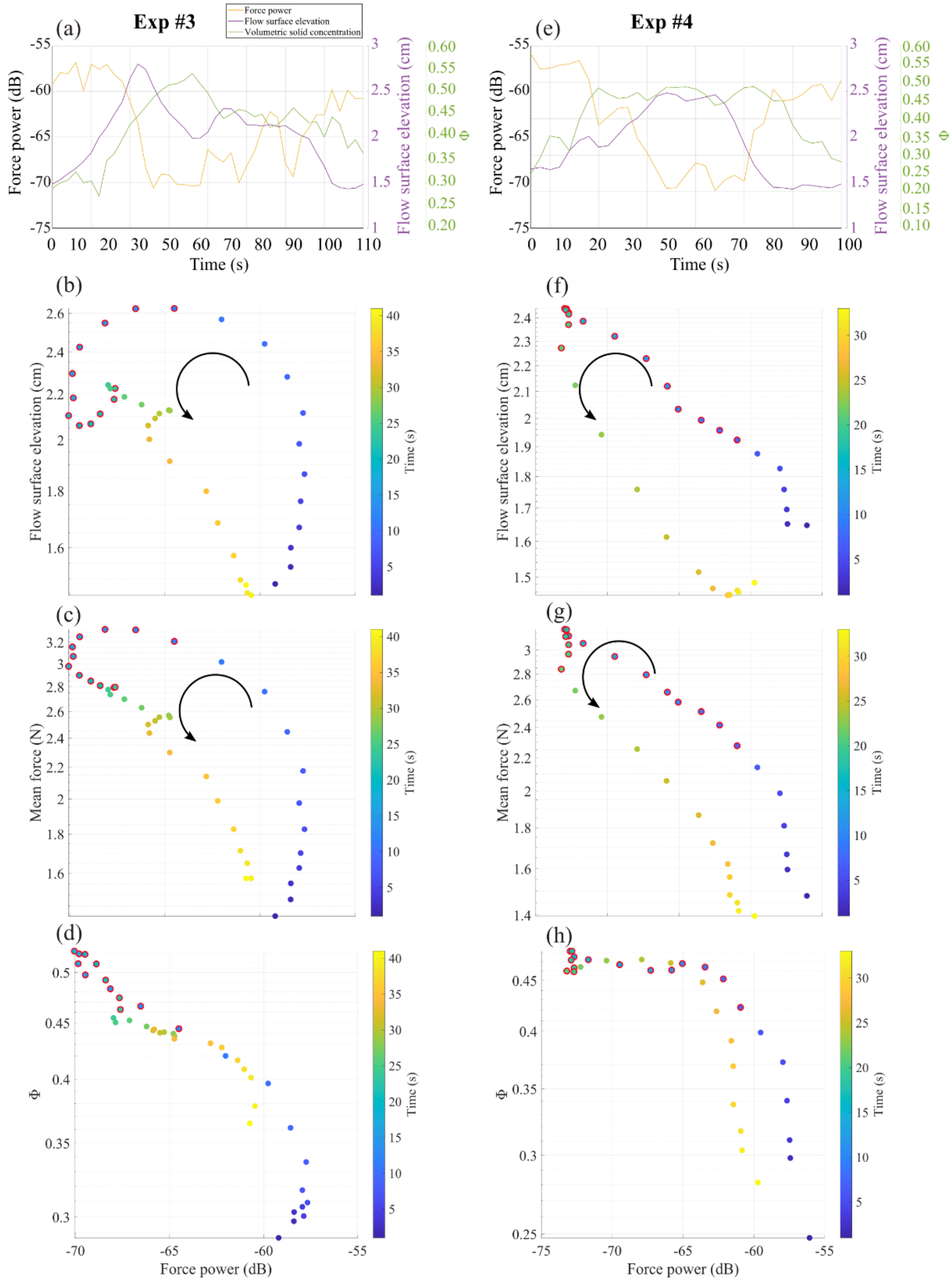

Figure S4. All the panels of Figure S4 refer to the time intervals between the vertical dashed red lines in Figure S3b and S3f. Figure S4a and S4e show the evolution in time of the force power, flow surface elevation, and volumetric solid concentration associated with the highly concentrated sediment flows, while the log-log scatterplots of Figure S4b-c-d and Figure S4f-g-h have force power on the x axis and flow properties on the y axis, where dots' color changes with time. As stated in the main text, we are able to identify the time interval when the content of fine sediments is maximum. These moments are marked in the scatterplots with circled dots. All the measurements are smoothed on a time window of 5 sec.

Text S6. The control of the coarse fraction of the sediment mixture on force fluctuations

Tsai et al. (2012) propose that the seismic signal P generated by a sediment flow is directly related to two main geometric parameters of the flux, i.e. the number of particles n and the mass m (i.e. the diameter) of them, and two dynamic parameters, which are the rate of impact $1/t_i$ and the impact velocity w_i. Their model can be written as:

$$P \sim \frac{n}{t_i} m^2 w_i^2 \quad (1)$$

The model is built under simplistic assumptions, but it can be adopted to better understand the influence of each of these parameters on the generation of seismic power. As we are interested in investigating the role of the particle diameter, we express the seismic power as a function of the mass, under the assumption that the other parameters (i.e. n, $1/t_i$, and w_i) do not depend on the grain size. If we further consider that the mass of the particle is proportional to the third power of the particle diameter, we can rewrite equation 1 in the form:

$$P = \int p(D)\ D^6 dD \quad (2)$$

where p(D) is the percentage of grains of diameter D. The seismic power for phase I, II, and III is shown in Figure S7. We can observe that in the frequency range of interest ($100 - 2500$ kz) the coarse fraction of the sediment flow generates most of the seismic power. For each phase most part of the seismic power is always related to the coarse fraction of the flux. Although phase II can reach high contents of fines (~ 30 %), their contribution to seismic power is low. The contribution of particle diameters of 4 mm is 12 dB lower than that of particles of 8 mm.

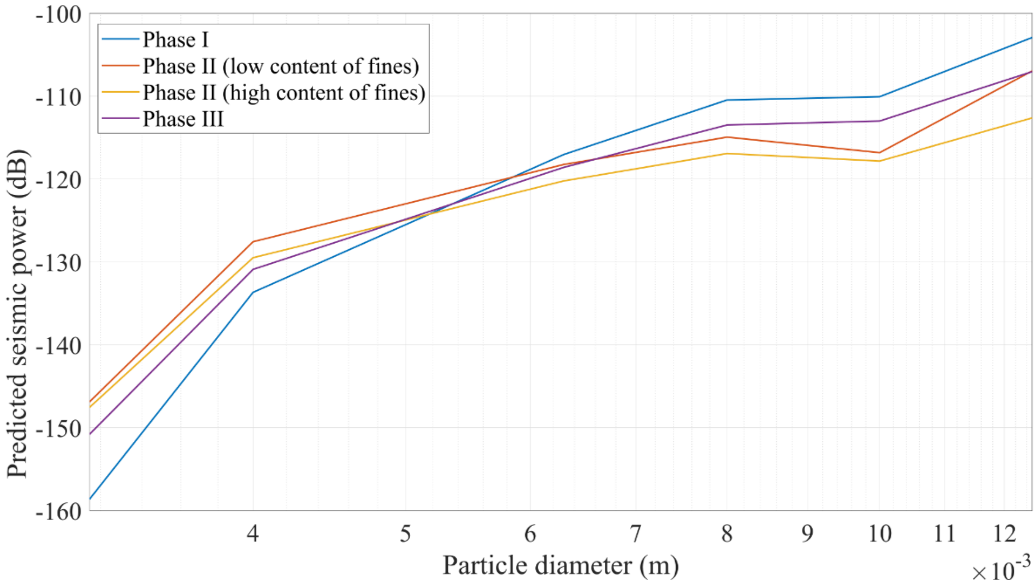

Figure S5. Predicted seismic power as a function of particle diameter following Tsai et al. (2012). Predictions are shown for each phase in a log-log plot. Particle diameters are truncated at 3.15 mm since the contribution of smaller particles is negligible.

Text S7. Changing the moving average window size

In Figure S6 we show the equivalent of Figure 3 from the main text but with a moving average window size of 2 s instead of 5 s. We observe that the hysteresis behaviour remains clear for flow surface elevation and mean force against force power (Figure S6a-b and Figure S6d-e), while the rising and falling limbs of volumetric solid concentration collapse on a unique curve (Figure S6c and Figure S6f). These observations confirm that the small clockwise hysteresis showed in Figure 3b and Figure 3f is not significant.

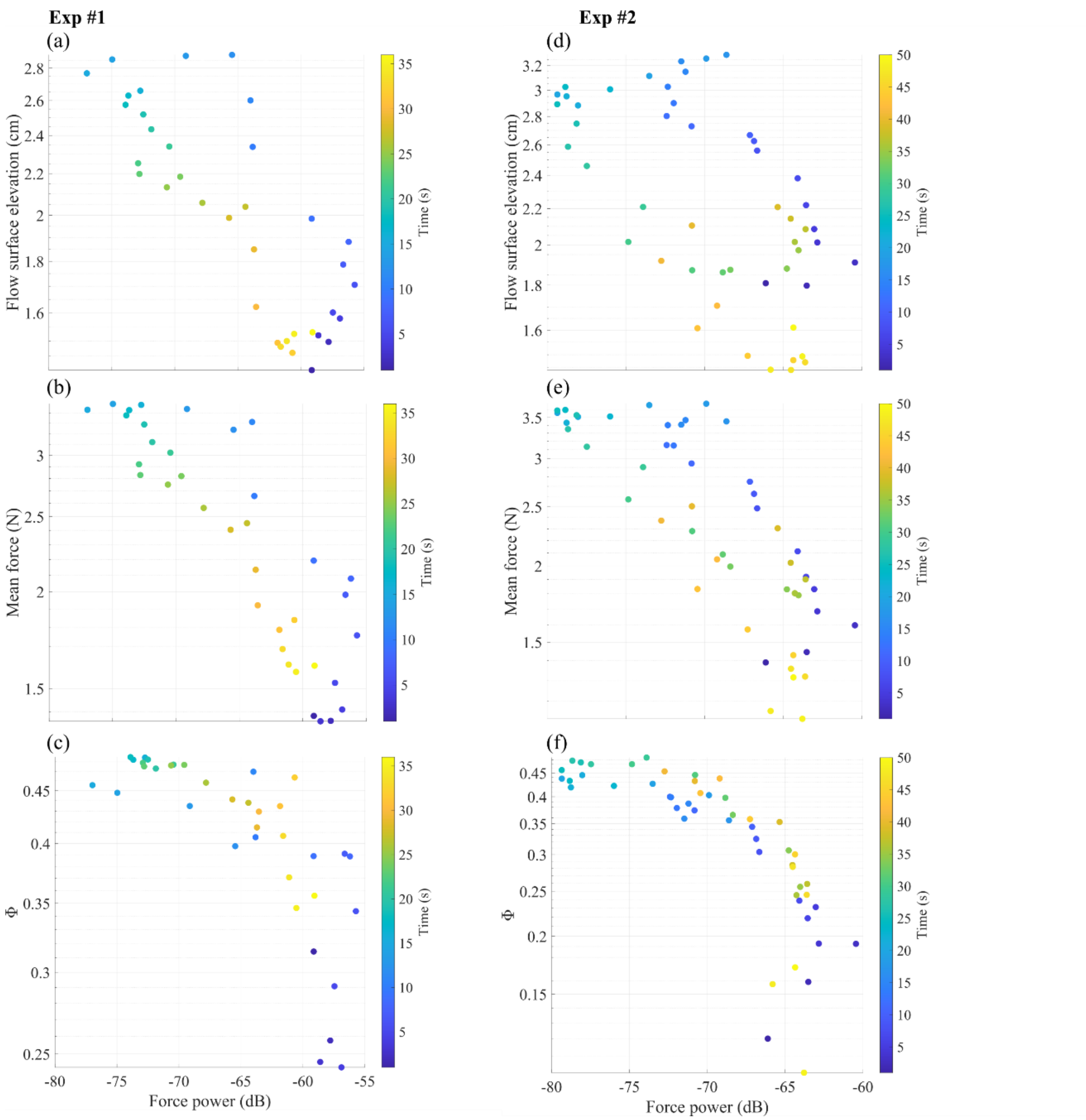

Figure S6. All the panels of Figure S6 refer to the time intervals between the vertical dashed red lines in Figure 2f and 2j. The log-log scatterplots of Figure S6a-b-c and Figure S6d-e-f have force power on the x axis and flow properties on the y axis, where dots' color changes with time. All the measurements are smoothed on a time window of 2 sec.

Movie S1. Movie S1 is from the webcam installed above the force plate. It refers to Exp #2.

Movie S2. Movie S2 is from the camera installed close to the upstream piezoelectric sensor. It refers to Exp #2.